MIT Libraries | DSpace@MIT

MIT Open Access Articles

Transcriptional regulatory dynamics drive coordinated metabolic and neural response to social challenge in mice

Massachusetts Institute of Technology

Research

Transcriptional regulatory dynamics drive coordinated metabolic and neural response to social challenge in mice

Michael C. Saul,[1,12] Christopher H. Seward,[1,2,12] Joseph M. Troy,[1,3] Huimin Zhang,[1,2] Laura G. Sloofman,[1,4] Xiaochen Lu,[1,2] Patricia A. Weisner,[1,5] Derek Caetano-Anolles,[1,2] Hao Sun,[1] Sihai Dave Zhao,[1,6] Sriram Chandrasekaran,[7,8,9] Saurabh Sinha,[1,4,10,11] and Lisa Stubbs[1,2,5]

[1]Carl R. Woese Institute for Genomic Biology, University of Illinois at Urbana–Champaign, Urbana, Illinois 61801, USA; [2]Department of Cell and Developmental Biology, University of Illinois at Urbana–Champaign, Urbana, Illinois 61801, USA; [3]Illinois Informatics Institute, Urbana, Illinois 61801, USA; [4]Center for Biophysics and Quantitative Biology, University of Illinois at Urbana–Champaign, Urbana, Illinois 61801, USA; [5]Neuroscience Program, University of Illinois at Urbana–Champaign, Urbana, Illinois 61801, USA; [6]Department of Statistics, University of Illinois at Urbana–Champaign, Urbana, Illinois 61801, USA; [7]Harvard Society of Fellows, Harvard University, Cambridge, Massachusetts 02138, USA; [8]Faculty of Arts and Sciences, Harvard University, Cambridge, Massachusetts 02138, USA; [9]Broad Institute of MIT and Harvard, Cambridge, Massachusetts 02142, USA; [10]Department of Computer Science, [11]Department of Entomology, University of Illinois at Urbana–Champaign, Urbana, Illinois 61801, USA

Agonistic encounters are powerful effectors of future behavior, and the ability to learn from this type of social challenge is an essential adaptive trait. We recently identified a conserved transcriptional program defining the response to social challenge across animal species, highly enriched in transcription factor (TF), energy metabolism, and developmental signaling genes. To understand the trajectory of this program and to uncover the most important regulatory influences controlling this response, we integrated gene expression data with the chromatin landscape in the hypothalamus, frontal cortex, and amygdala of socially challenged mice over time. The expression data revealed a complex spatiotemporal patterning of events starting with neural signaling molecules in the frontal cortex and ending in the modulation of developmental factors in the amygdala and hypothalamus, underpinned by a systems-wide shift in expression of energy metabolism-related genes. The transcriptional signals were correlated with significant shifts in chromatin accessibility and a network of challenge-associated TFs. Among these, the conserved metabolic and developmental regulator ESRRA was highlighted for an especially early and important regulatory role. Cell-type deconvolution analysis attributed the differential metabolic and developmental signals in this social context primarily to oligodendrocytes and neurons, respectively, and we show that ESRRA is expressed in both cell types. Localizing ESRRA binding sites in cortical chromatin, we show that this nuclear receptor binds both differentially expressed energy-related and neurodevelopmental TF genes. These data link metabolic and neurodevelopmental signaling to social challenge, and identify key regulatory drivers of this process with unprecedented tissue and temporal resolution.

[Supplemental material is available for this article.]

Agonistic encounters represent challenges to wellbeing and require a swift, measured response. Animals must learn quickly from socially threatening situations and adjust their behavior during future encounters accordingly; failure to adapt can have serious consequences. Counterbalancing the necessity for normal fear reactivity are the physiological costs of a reaction: Repeated exposure to social challenge adversely impacts neurochemistry, behavior, and health in both recipients and perpetrators of threats (Hawker and Boulton 2000; Bjorkqvist 2001).

Though social challenges have stronger and more durable consequences when reinforced, neurochemical and behavioral differences are observed after even a single challenge. For instance, one round of the classic "resident-intruder" territorial challenge test is sufficient to rapidly raise blood glucose and serum corticosterone in both naïve residents and intruder mice while inducing alterations in neurochemistry associated with depressive and anxious behaviors (Meehan et al. 1987; Audet et al. 2010). Such a response triggers the first steps in fear learning, preparing an animal for future encounters by tempering subsequent behaviors (Duvarci and Pare 2014). Normal learning from social challenge is critical to establishing social rank, a ubiquitous element of social hierarchies across metazoans (Fernald and Maruska 2012), while abnormalities in social threat-based learning lead to maladaptive behaviors, including those associated with human neuropsychiatric disease (for reviews, see Pittenger 2013; Gilmartin et al. 2014).

Fear learning in response to social challenge is ubiquitous across metazoans, and our recent study demonstrated deeply conserved molecular mechanisms underlying the early steps in this response (Rittschof et al. 2014). These previous results documented rapid activation of closely related genes and strikingly similar pathways in brains of three classic behavioral models—honey bees, stickleback fish, and laboratory mice—very shortly after challenge exposure. These data revealed a rapid down-regulation of genes involved in oxidative phosphorylation, correlated with the activation of a conserved cohort of coexpressed neurodevelopmental transcription factors (TFs) and signaling pathways. The results suggested that energy metabolism and neurodevelopmental systems cooperate as central parts of a deeply conserved mechanism involved in coordinating behavioral plasticity and, ultimately, emotional learning after social threat.

While our initial study suggested a link between metabolism and neural signaling through development, it did not include the tissue and temporal resolution needed to resolve this link, describe the downstream transcriptional response, or reveal the factors involved in its regulation. To understand the molecular response within the animal's brain as it responded to a salient social challenge and to identify the factors regulating these neuronal events, we generated and then computationally integrated data sets reflecting gene expression and chromatin states as they changed across the brain and over time.

Results

Gene expression analysis reveals a complex interplay of metabolic signaling and developmental regulators

A generalized linear model identifies the systems–wide response

Our previous study (Rittschof et al. 2014) focused on gene expression in resident and control animals in the ventral hypothalamus (HYP), sampling gene expression quickly (15 min) after removal of the intruder mouse. To further explicate this response and its downstream consequences, we examined gene expression at 30, 60, and 120 min after intruder removal in three interconnected brain regions with key roles in fear learning and response to aggression: frontal cortex (FCX), whole HYP, and amygdala (AMY) (for review, see Takahashi and Miczek 2014). A table summarizing the gene expression and other genomics data sets presented in this article is available as Supplemental Table S1.

To maximize the utility of this rich expression data set, we modeled the system-wide interplay of the transcriptional response across these three tissues and over time. We used a generalized linear model (GLM)—essentially a three-way factorial ANOVA, but with different distributional assumptions—to detect differential expression related to four factors (predictors) of interest: a factor indicating whether the sample came from a challenge or control animal (challenge),

factors representing the interaction between challenge and tissue assayed (tissue:challenge) or interaction between challenge and time point (challenge:time), and also the three-way interaction among all of the previous factors (tissue:challenge:time). Each factor provides different information about tissue and temporal patterning of response to social challenge, and each yielded many differentially expressed genes (DEGs) of interest at a false-discovery rate (FDR) < 0.10 (Supplemental Table S2).

The gene with the strongest P-value among challenge factor DEGs was $Ide,$ encoding insulin degrading enzyme (edgeR FDR = 6.70×10^{-5}) (Fig. 1A); mitochondrial tRNA gene $mt\text{-}Tq$ was highest ranked among tissue:challenge DEGs (edgeR FDR = 1.3×10^{-4}). However, functional analysis revealed no significant enrichments among DEGs in either of these factors (Supplemental Table S3). In contrast, all DEGs from factors with a temporal component were very highly enriched for functional terms related to mitochondria and oxidative phosphorylation, with the tissue:challenge:time DEGs being most highly enriched in this functional category, with the gene $Ndufa7,$ encoding a mitochondrial NAD dehydrogenase, having the smallest P-value (edgeR FDR = 1.2×10^{-5}) (Fig. 1B; Supplemental Table S2). As exemplified by the expression patterns of Ide and $Ndufa7$ (Fig. 1) and in agreement with our earlier study (Rittschof et al. 2014), the GLM analysis thus implies that a hallmark of the response to social challenge is the rapid down-regulation of oxidative phosphorylation, accompanied by up-regulation of insulin signaling, and, more generally, the modulation of energy metabolism across brain regions and time after challenge.

Pairwise comparisons reveal the spatiotemporal sequence of events

Pairwise post-hoc comparisons of gene expression between challenged and control animals provide a different perspective, revealing the specifics of response within each tissue and time point. In
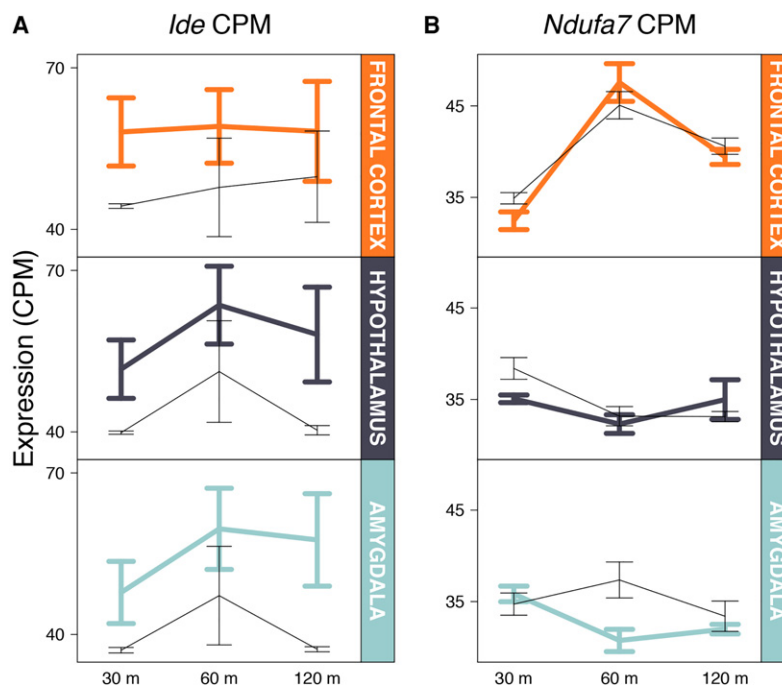

Figure 1. Expression patterns for Ide (A), the top DEG in the challenge factor of the GLM, and $Ndufa7$ (B), the top DEG in the tissue:challenge:time interaction factor of the GLM. Thin black lines are control samples, while thick colored lines are experimental samples. Error bars, SEM.

these comparisons, we found striking variation in the number of DEGs in different tissues over time (Fig. 2A; Supplemental Table S4). The transcriptomic response was most dramatic in FCX 30 min after challenge, while the largest responses in AMY and HYP occurred at 120 min. Though these DEG sets were mostly distinct, there were some important overlaps between tissues and time points (Fig. 2B,C). For example, *Ide*, the top gene associated with challenge in the factorial analysis (as described above), was consistently up-regulated in the HYP at all time points and up-regulated in all brain regions 120 min after challenge (Supplemental Table S4). Furthermore, the pairwise post-hoc comparisons generally overlapped with factors that included challenge in the model analysis (Supplemental Table S5).

To describe systems responses over time, we tested these pairwise post-hoc DEG sets for enrichment of Gene Ontology (GO) Biological Processes (BPs) and visualized the results using nonmetric multidimensional scaling (MDS) on distances derived from GO term semantic dissimilarity (Supek et al. 2011). This approach revealed a complex tissue-specific and temporal patterning of functional response (Fig. 2D; Supplemental Table S6). In FCX, an early up-regulation of GO BPs related to neurotransmission (a cluster

including a term related to insulin signaling), neuropeptide signaling, and learning was observed, which attenuated over the length of the experiment. In HYP, we detected a highly dynamic GO BP response over time, beginning with neuropeptide-related functions such as feeding behavior, followed by neural signaling and developmental functions. In AMY, few GO BPs were enriched in early time points, but strong, diverse enrichments were seen late after challenge. Similar to HYP, these functionally enriched categories ranged from neural signaling and transmission to development.

As a confirmation of the conclusions from the RNA-seq experiments, we performed RT-qPCR on a selection of key DEGs focusing on samples taken 120 min after social challenge. For each of these genes, we confirmed differential expression in the same direction and of the same approximate magnitude as in the RNA-seq study (Supplemental Fig. S1).

Taken together, the pairwise and system-wide expression analyses led to the hypothesis that early neuromodulatory signaling in FCX and HYP leads to a rapid shift in energy metabolism, which prefigures later neuronal plasticity in the amygdalar-hypothalamic axis. We explore this hypothesis further in following
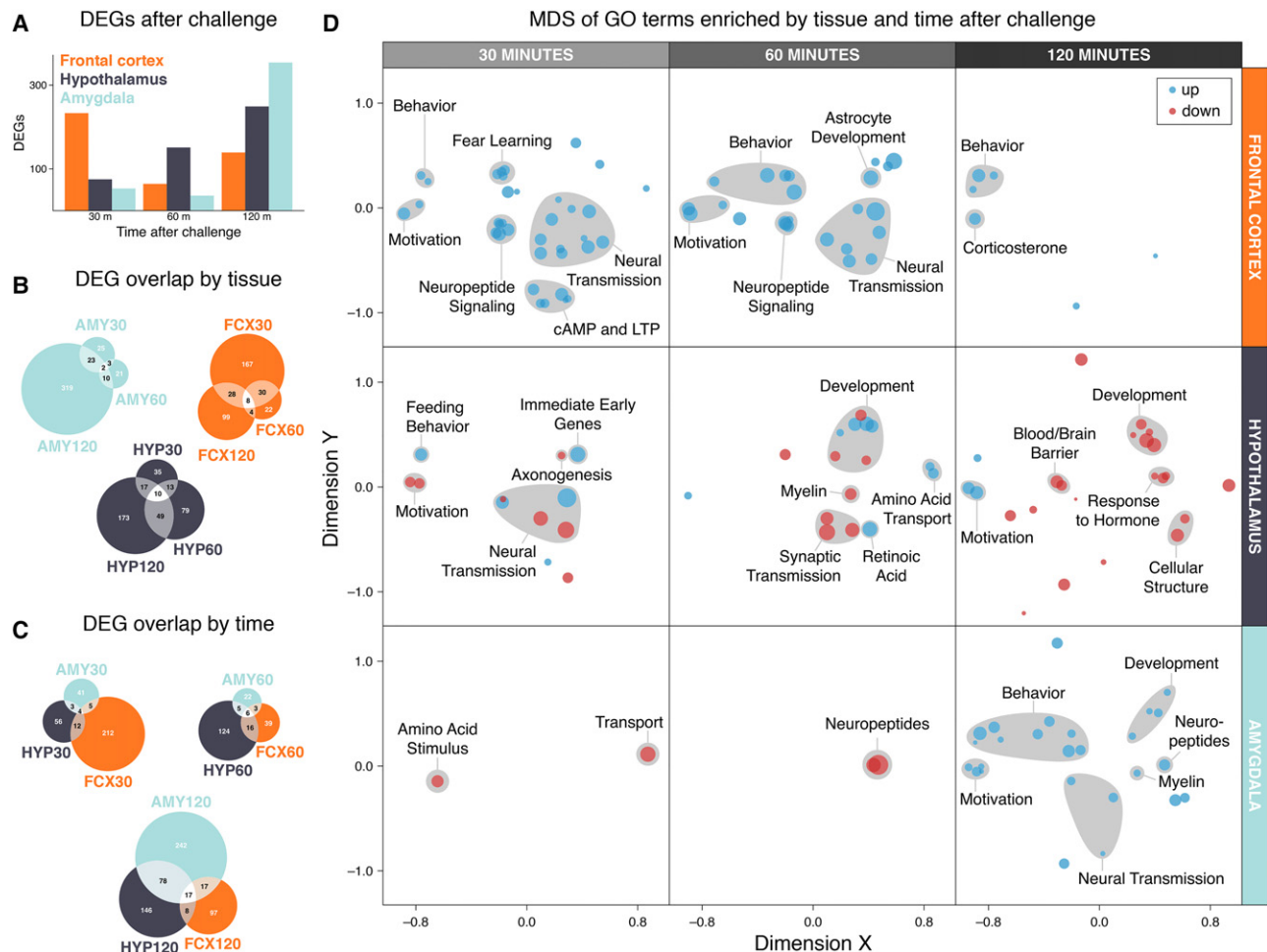
Figure 2. DEGs at FDR < 0.10 in the intruder versus control comparison for each combination of brain region and time point after intruder. (*A*) Plot of DEGs by time point after intruder. (*B*) Plots of overlap between time points after intruder within each brain region. (*C*) Plots of overlap between brain regions within each time point after intruder. (*D*) Semantic MDS plot projecting the spatial and temporal pattern of enriched GO biological processes (BPs). Distances represent GO semantic dissimilarity as measured by simRel. Point size represents log-fold-change of a GO BP term. Point color represents direction of differential expression of a GO BP term.

sections, but first we sought to associate these different transcriptomic signals to specific cell types across the brain.

Computational deconvolution analysis identifies cell–type–specific functions

Brain tissue is a complex mixture of cell types, complicating the interpretation of expression results. When we examined the overlap between our data set and genes linked to specific cell types in a previous RNA-seq experiment involving sorted mouse brain cells (Zhang et al. 2014), we found an enrichment of neuron-specific genes for most DEG sets, along with other cell types in specific brain regions and time points (Supplemental Table S7A). However, being limited to direct overlaps, this analysis included a relatively small subset of genes. To permit a more comprehensive analysis, we used "population-specific expression analysis" (PSEA) to deconvolve the signals from individual cell types in our data set (Kuhn et al. 2011). By using the same data set cited above (Zhang et al. 2014), we constructed reference signals for five different cell types: astrocytes, neurons, oligodendrocytes, microglia, and endothelial cells. We then classified DEGs from the GLM and from the pairwise post-hoc results based on these PSEA-defined cell categories. Because the reference data set utilized cortical tissue, we expect cell-type deconvolution to perform best on the FCX samples.

PSEA revealed strong overlaps between the pairwise post-hoc DEGs and genes associated with neurons from the reference data set (Supplemental Tables S7C, S8). In contrast, we identified significant overlaps between genes differentially expressed in the chal-

lenge-related GLM factors and genes associated with glia, most consistently oligodendrocytes, in all brain regions (Supplemental Tables S7D, S8). From these analyses, we infer that the system-wide energy metabolism shift detected by the GLM is correlated most highly with gene expression in oligodendrocytes, while the signals related to neuronal transmission and developmental pathways described in the post-hoc analysis derive primarily from neurons.

Coexpression reveals the organization of oxidative phosphorylation and neuronal signaling genes in opposing network clusters

To evaluate the interrelationships between genes and functions underlying challenge response, we used weighted gene correlation network analysis (WGCNA) to generate a coexpression network across tissues and time points (Supplemental Table S9). To visualize the most stable coexpression relationships, we extracted network edges with correlation coefficients ≥0.85 in absolute value and with the same sign in every tissue. The resulting high-correlation network displayed a topology wherein two distinct gene clusters were bridged by a strong predominance of anticorrelated edges (Fig. 3A). The opposing "left" (L) and "right" (R) gene clusters were very highly enriched in functionally related genes; the L cluster predominates in functions related to oxidative phosphorylation, while the R cluster is especially enriched in genes related to transcriptional regulation and neuronal signaling (Supplemental Table S9).
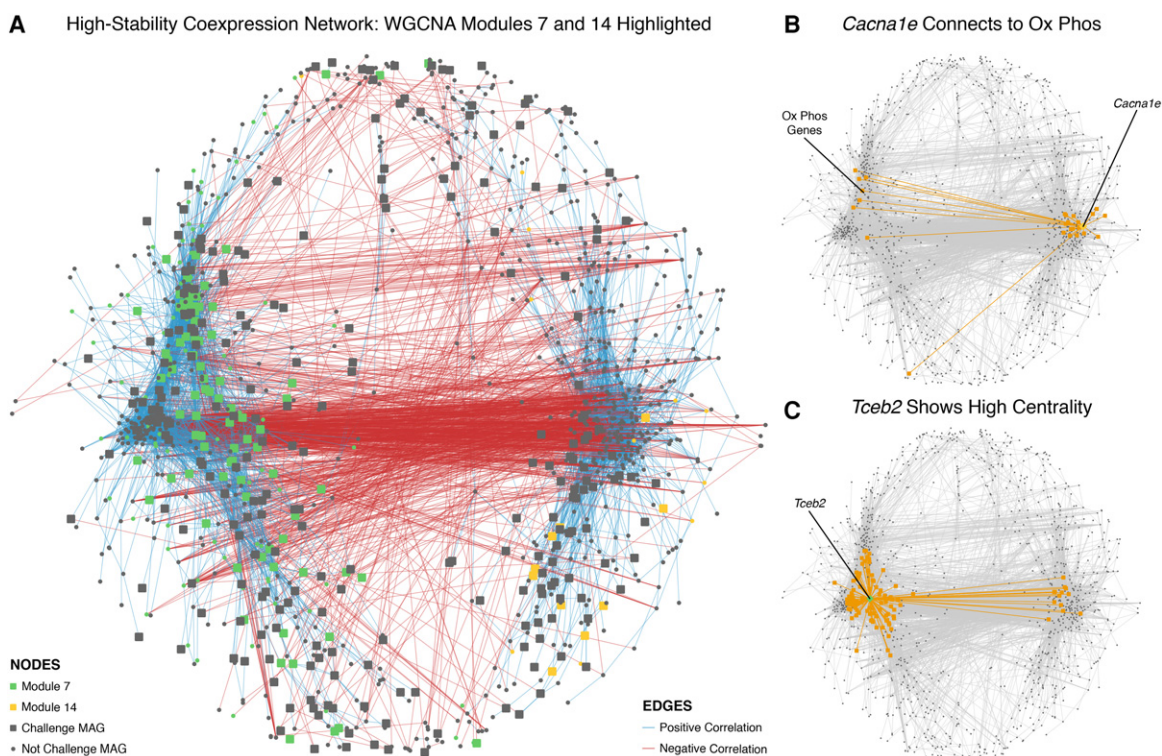
Figure 3. (A) Coexpression network of plotting the largest connected component with all relationships with correlations of an absolute value of 0.85 or better. The network topology includes two sides connected by a profusion of negative correlations. Module 7 nodes (green), which are associated with oxidative phosphorylation, inversely connect to module 14 nodes (yellow), which are associated with ion channels. (B) The gene with the highest betweenness centrality in module 14, *Cacna1e*, connects to many oxidative phosphorylation genes. Edges connecting out from *Cacna1e* and the nodes they connect to are highlighted in orange. (C) The gene with the highest betweenness centrality in module 7, *Tceb2*, implies a role for transcriptional regulatory dynamics. Edges connecting out from *Tceb2* and the nodes they connect to are highlighted in orange.

Within this network structure, we identified two WGCNA modules with particularly significant relationships to social challenge, modules 7 and 14, whose eigenegenes are strongly anticorrelated ($r = -0.90$). High-stability module 7 genes were highly enriched for oxidative phosphorylation, while high-stability module 14 genes were enriched for ion channel activity. Indeed, the gene with the highest measure of betweenness centrality (BC; a metric of network connectivity) from module 14, *Cacna1e*, is a DEG in the tissue:challenge:time factor and in FCX pairwise analysis at 30 min and displays very strong and direct negative relationships with oxidative phosphorylation-related nodes (Fig. 3B). *Cacna1e* is particularly interesting in this context, connecting calcium signaling, insulin signaling, and synaptic plasticity (Pereverzev et al. 2002; Breustedt et al. 2003), and has been implicated in fear learning (Lee et al. 2002). The WGCNA network structure thus identified concrete bridges between the metabolism-related DEGs described in the GLM results and the neural signaling DEGs described in the pairwise post-hoc results, providing an explicit architecture of an oppositional relationship between brain oxidative phosphorylation and the neuronal response to social challenge.

We further identified the gene with the highest BC in module 7 and in the entire network structure as *Tceb2*, a subunit of the TF B complex that activates RNA Pol II activity (Fig. 3C). Together, the central role of *Tceb2* in core transcription and the enrichment of TFs and chromatin modifiers in the L cluster imply that transcriptional regulation is a core component of the network, a prediction examined further below.

Figure 4. Network of TFs with TF–TF interactions in the TRN highlighting tissue-specific and time-specific regulators. TFs whose targets were enriched for DEGs in FCX are orange, TFs whose targets were enriched for DEGs in HYP are dark gray, and TFs whose targets were enriched for DEGs in AMY are blue. The times after social challenge where enrichment was found are depicted as shapes: Square nodes are enriched at 30 min, circular nodes are enriched at 120 min, and diamond-shaped nodes are enriched at both 30 min and 120 min after challenge. Multicolored TF modules such as *Pparg* and *Lhx2* were enriched for DEG in multiple regions or time points. TFs that were not enriched for any tissue-specific or time-specific DEG—shown as small nodes—may represent homeostatic processes active across all conditions.

Transcriptional regulatory dynamics underlie the transcriptomic response to intruder

Transcriptional regulatory network reconstruction identifies a cohort of TFs central to intruder response

To identify TFs orchestrating this challenge response, we reconstructed a transcriptional regulatory network (TRN) across the expression data set using the ASTRIX approach. ASTRIX is also based on coexpression but centers on expressed TFs and highly correlated putative "target genes" (Chandrasekaran et al. 2011). The analysis yielded a TRN consisting of 4251 interactions between 253 TFs and 1211 target genes (Supplemental Table S10). We validated this TRN by comparing TF–gene interactions in our TRN with those constructed using DNase footprinting from the ENCODE Project (Stergachis et al. 2014), and found highly significant overlap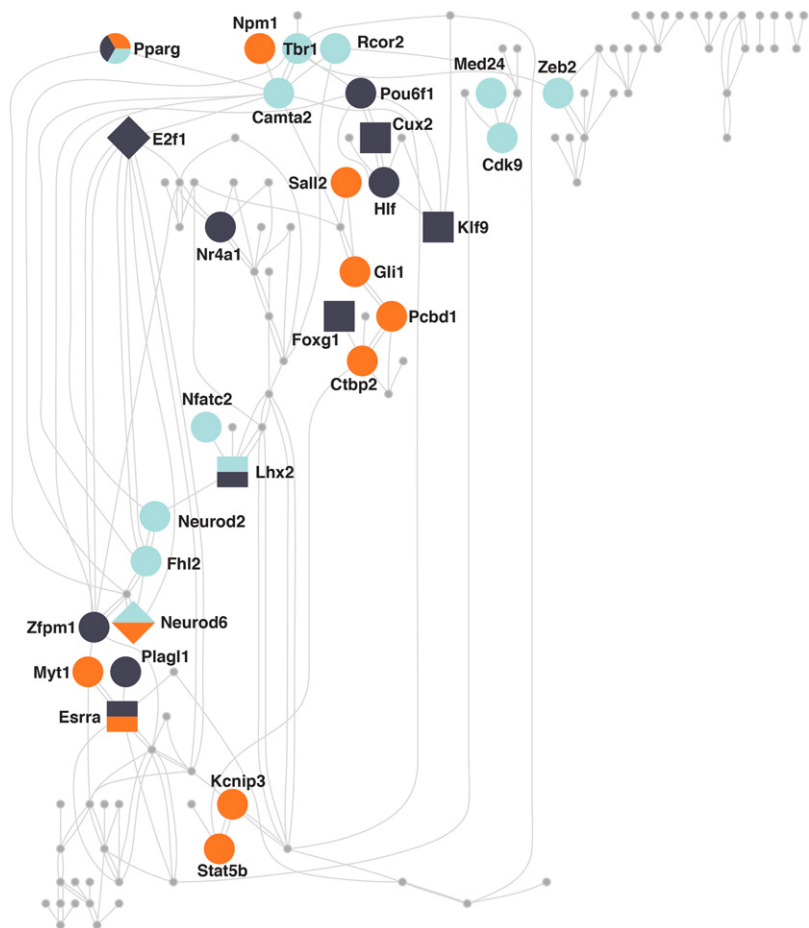 between networks constructed using ENCODE data from mouse adult and fetal brains (hypergeometric overlap test P-values $<10^{-11}$) compared with a random brain TRN with the same TFs and targets (for further details, see Supplemental Methods).

To identify the TFs most likely to drive the observed differential gene expression, we extracted those TFs with predicted target sets enriched in pairwise and model DEGs (Supplemental Table S11; pairwise results presented in Fig. 4). The TRN noted above includes TFs with related functions and outlines a regulatory architecture linking energy metabolism, developmental signaling, neuron plasticity, and social behavior (Table 1). Especially noteworthy is the presence of TFs associated with combined metabolic and behavioral phenotypes including ESRRA, PLAGL1, NR4A1, and NFATC2.

Significant global chromatin remodeling accompanies intruder response

Gene expression patterns integrate TF activity with chromatin accessibility, and the magnitude and rapidity of the challenge-

Saul et al.

Table 1. Metabolic and neurological functions for TFs in the social challenge TRN

Function	TF genes	References
Neuropeptide signaling	*Foxg1, Stat5b, Pparg*	Buonfiglio et al. (2015); Garretson et al. (2015); Frullanti et al. (2016).
Insulin, glucose homeostasis, oxidative phosphorylation	*Esrra, Pparg, Nfatc2, Nr4a1, Fhl2, Plagl1, Pcbd1*	Bayle et al. (2002); Savage et al. (2002); Yang et al. (2006); Dufour et al. (2011); Hoffmann and Spengler (2012); Perez-Sieira et al. (2014); Li et al. (2015).
Wnt pathway	*Esrra, Pparg, Nfatc2, Fhl2, Ctbp2, Tbr1*	Murphy and Hughes (2002); Valenta et al. (2003); Auld et al. (2012); Papachristou et al. (2014); Li et al. (2015); Wang et al. (2015).
Neuron differentiation, neurite outgrowth and synaptic plasticity	*Neurod2, Neurod6, Nr4a1, Nfatc2, Sall2, Tbr1, Cux2, Foxg1, Klf9, E2f1, Zeb2, Rcor2, Plagl1*	Schwab et al. (2000); Graef et al. (2003); Pratt et al. (2004); Abrajano et al. (2009); Pincheira et al. (2009); Scobie et al. (2009); Cubelos et al. (2010); Suzuki et al. (2011); McKinsey et al. (2013); Chen et al. (2014); Huang et al. (2014); Adnani et al. (2015).
Social behavior, emotional learning	*Esrra, Neurod2, Tbr1, Gli1*	Lin et al. (2005); Huang et al. (2014); Cui et al. (2015); Hung et al. (2015a,b); Notwell et al. (2016).

associated transcriptional response suggested that shifts in chromatin accessibility might underlie this response. Since accessible chromatin is generally marked by histone H3 acetylated at lysine 27 (H3K27ac) (Hon et al. 2009), we carried out chromatin immunoprecipitation followed by deep sequencing (ChIP-seq) with a validated H3K27ac antibody to map accessible chromatin in each brain region at different time points after challenge (Supplemental Table S12). We will refer to H3K27ac peaks shared by challenged and control animals as "baseline peaks" and peaks significantly altered in accessibility after challenge as "differential accessibility peaks" (DAPs).

We identified 23,763 DAPs with at least a twofold difference in H3K27ac enrichment (at HOMER $P < 1 \times 10^{-4}$) between challenged and control samples among all comparisons (Supplemental Table S12). Chromatin near DEGs generally transitioned from an open to a relatively more closed state after challenge in both FCX and HYP, while chromatin transitioned to a more open state in AMY samples over time, a pattern that mirrors the changes seen in expression (Fig. 5A; Supplemental Table S12). Despite the apparent match between accessibility and expression profiles, DAPs did not track pairwise post-hoc differential expression in matched regions and times after social challenge (Supplemental Table S13A).

We attribute this mismatch to two general processes. First, we believe there may be a mismatch in the speed of changes in accessibility and in changes in expression. For example, the only brain region in which DAPs significantly predict pairwise DEGs is the AMY, where genes near DAPs at 30 min after social challenge predict DEGs at 120 min after challenge (hypergeometric overlap test, FDR = 1.61×10^{-8}). Therefore, DAPs detected at 120 min after challenge—by far the most numerous—may predict gene expression at later time points. Second, while baseline H3K27ac peaks generally clustered near promoters (41.2% of baseline H3K27ac peaks lie within 5 kb upstream of and 2 kb downstream from transcription start sites), DAPs in every brain region and time point displayed a highly significant preference for more distal locations relative to baseline peaks (Fisher's exact test P-values $<10^{-76}$) (Fig. 5B; Supplemental Table S13B). Therefore, although it is more difficult to assign distal enhancers to target genes conclusively, correlations limited to promoter-proximal DAPs are likely to miss many significant regulatory relationships.

To identify cases of potentially causative links between differential accessibility and expression, we examined DAPs within longer distances (100 kb) of the TSS of the closest pairwise DEGs. We found 788 DAPs linked to 323 DEGs across brain regions and time

points after social challenge (Supplemental Table S14). Among these DAPs were known distal enhancers, including an element located approximately 10 kb downstream from the immediate early gene *Fos* (Fig. 5C). This distal element, called "e5," interacts with the *Fos* promoter through 3D chromatin interactions in response to neuronal stimulation of various types (Joo et al. 2016). Together these data suggest that the modulation of distal enhancers and the three-dimensional chromatin landscape are hallmarks of the social challenge response.

Motif enrichment within open chromatin regions reveals a role for pioneer factors and highlights ESRRA activity in intruder response

To explicate the interaction between active TFs and chromatin components, we asked whether known TF binding motifs (TFBMs) were enriched in baseline chromatin near DEGs or in DAP-DEGs. Although we did not find many DAPs near TSS positions, the highest density of baseline H3K27ac peaks was found near TSS positions. We examined motifs within −5-kb to +2-kb intervals, filtering data to include only motifs present in baseline-accessible regions within these intervals. By using this filter, we found significant enrichment of TFBMs, including motifs for TFs in the TRN (Supplemental Table S15A). For example, DEGs for HYP and FCX showed enrichment for ESRRA-related motifs, particularly in DEGs down-regulated at 60 min. Importantly, we did not detect significant TFBM enrichments without first filtering for accessibility; limiting motif searches to accessible windows thus greatly improved the accuracy of TFBM identification.

Focusing next on DAP-DEGs, we identified significant motif matches (binomial test P-value <0.001) primarily to "pioneer factors" (for review, see Iwafuchi-Doi and Zaret 2014), including TFAP2A, CEBPA, POU3F1, and MEIS1. We also identified enrichments for TFBMs associated with chromatin remodeling factors (HINFP1 [Ng et al. 1999]; ELK1 [Besnard et al. 2011]; EGR1 [Spaapen et al. 2013]) (Supplemental Table S15B). We regard these statistical associations as evidence that the regulatory response to challenge includes the action of pioneer and remodeling factors to reshape the accessibility landscape near target genes.

The combined analysis of gene expression, chromatin accessibility, network reconstruction, and DNA binding motif enrichment revealed several apparent mechanisms through which TFs and other key proteins participate in the challenge response (Table 2). For example, while the abundance of some TFs, like *Fos* and *Neurod2*, appears to be regulated transcriptionally, the differential expression may or may not be driven through differential accessibility. On the other hand, for TFs such as ESRRA whose nuclear location and DNA

binding activities are regulated post-translationally (Rossi et al. 2011; Huss et al. 2015), their central action in the TRN appears without differential expression of the genes themselves.

ESRRA protein binds to promoters of metabolically active genes in FCX

A central hypothesis to emerge from these studies is that the adaptive response to social challenge couples the down-regulation of brain oxidative phosphorylation to the activation of pathways associated with neuronal plasticity. Our data further indicate that this transcriptional response is correlated with alterations in the chromatin landscape coordinated with the activities of specific TFs. At the nexus of these expression and regulatory dynamics stands the TF ESRRA, a nuclear receptor known as a key regulator of metabolism and differentiation (for review, see Villena and Kralli 2008). Also highlighted in our cross-species study (Rittschof et al. 2014), ESRRA was implicated in both the TRN and baseline motif predictions presented here. Of particular interest, ChIP-chip experiments involving human cell lines (Deblois et al. 2009) and mouse heart and liver (Dufour et al. 2007; Charest-Marcotte et al. 2010) indicate that ESRRA is a direct regulator of energy metabolism genes. Consistently, *ESRRA* mutations are associated with both metabolic defects and social behavior deficits in humans and mice (Cui et al. 2015), suggesting a central role for ESRRA in coordinating metabolic and behavioral response.

We tested a key provision of this hypothesis by performing ESRRA ChIP-seq in FCX chromatin collected 30 min after challenge, identifying 636 ChIP-seq peaks (Supplemental Table S16). ChIP peaks were strongly enriched for the known ERRE motif shared by ESRRA and paralogs (HOMER ESRRB motif enrichment P-value: 1×10^{-356}) and included a number of previously identified ESRRA binding targets. Notably, one of the strongest peaks, mapped near the *Esrra* promoter, marks a conserved multi-hormone response element that binds ESRRA and other nuclear receptors (Laganiere et al. 2004; Liu et al. 2005), indicating auto-regulation.

Analysis of genes nearest ESRRA ChIP-seq peaks showed especially high enrichment for mitochondrial and oxidative phosphorylation-related functions (DAVID annotation cluster scores = 26.95 and 14.85), as well as terms related to glycolysis and gluconeogenesis. Genes near ESRRA peaks were also highly enriched in DEGs from the tissue:challenge:time factor of the GLM results (hypergeometric overlap test P-value = 0.0053). Aside from energy metabolism genes, ESRRA FCX binding sites were enriched near TF loci; these include DEGs such as the genes encoding known ESRRA interactor and energy metabolism regulator GABPA and the TRN component and neurodevelopmental TF NEUROD2 (Supplemental Table S16; Sakkou et al. 2007). These data suggest that *Esrra* is central to the challenge-relat-

ed response and potentially involved in coordinating the regulation of energy metabolism genes with expression of neurodevelopmental TFs.

ESRRA is highly expressed in oligodendrocytes and neurons in FCX

Determining where and when a gene or protein is expressed is central to deciphering its biological function, and ESRRA is a case in point. A recent study ruled out expression of mouse ESRRA in cortical astrocytes and concluded that the protein was neuronal, but did not examine markers to test this assumption (Cui et al. 2015). Furthermore, the cell-type–specific expression data upon which the PSEA model was based showed *Esrra* gene expression in multiple cortical cell types (Zhang et al. 2014). Since PSEA analysis tied the energy metabolism signal primarily to oligodendrocytes in the FCX, we hypothesized that ESRRA would also be expressed in that cell type.

To test this hypothesis, we used an antibody for ESRRA together with those for two cell-type–specific markers: CNPase (a marker of oligodendrocyte cytoplasm) and NeuN (a marker of neuronal nuclei) in immunohistochemistry on thick (200-μm) CLARITY-cleared mouse brain slices. ESRRA protein was expressed at high levels in the nuclei of cells across the cortex (Fig. 6A). Like many TFs and most nuclear receptors (Rossi et al. 2011), ESRRA was also present in the cytoplasm, including cellular processes. High-magnification images revealed ESRRA protein expression in oligodendrocyte nuclei, identified by being surrounded by thin layers of
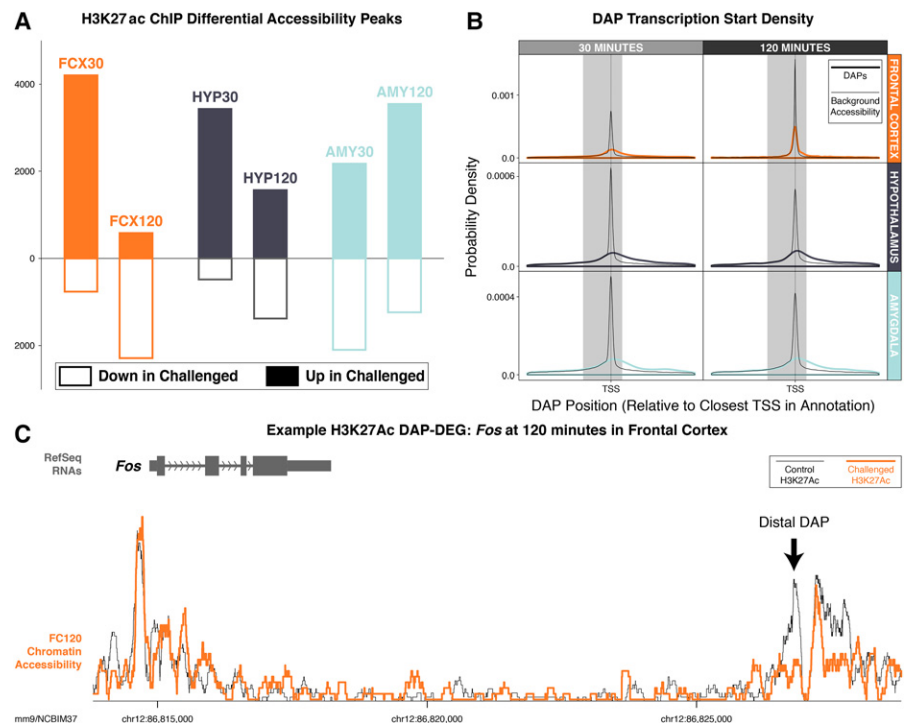
Figure 5. (*A*) H3K27ac DAPs in pairwise comparisons at a threshold of twofold. Solid bars *above* the *x*-axis represent peaks with increased accessibility in experimental samples relative to control. Outlined bars *below* the *x*-axis represent peaks with decreased accessibility in experimental samples. (*B*) Probability density of locations of differential accessibility in a 30-kb window around TSS sites. While the highest density of DAPs still lies within 5 kb upstream of or 2 kb downstream from (gray boxes) the TSS, the majority of DAPs are distal. Relative to background accessibility (thin black lines), DAPs have lower density near the TSS and higher density at distal sites. (*C*) Example distal differential accessibility peak in a known distal enhancer element for the immediate early gene *Fos* in FCX at 120 m after challenge.

Table 2. Summary of key genomics results for selected genes reveals different modes of activation and participation in the challenge response

Gene	Model DEG		Pairwise DEG		DAP association[a]		TRN:target enrichment		Promoter/DAP Motif enrichment[b]		ESRRA target
	Factor	FDR	Data set[c]	FDR	Data set[c]	p	Date set[c,d]	FDR	Data set[c]	FDR	
Esrra	–	–	–	–	–	–	HYP30	0.0039	HYP60	0.046	Y
							HYP-All	0.0090	FCX30	0.080	
							FCX-All	0.046			
Srf	–	–	–	–			All-120	0.0018	HYP60	0.0028	
Foxg1	–	–	HYP30	6.2×10^{-6}	HYP30	2.1×10^{-9}	HYP30	2.0×10^{-4}	HYP60	0.046	–
			HYP60	7.8×10^{-3}	–	–					
			–	–	HYP120	1.7×10^{-5}					
Fhl2	–	–	AMY120	0.089	–	–	AMY120	8.7×10^{-4}	NA	–	Y
Myt1	Tissue:Challenge:Time	–	FCX30	0.068	–	–	FCX-All	0.002	–	–	Y
							FCX120	0.003			
Nr4a1	–	–	HYP30	0.0011	–	–	HYP-All	4.6×10^{-4}	HYP30	0.005	–
Neurod2	–	–	–	–	AMY30	8.0×10^{-7}	AMY-All	2.2×10^{-5}	–	–	Y
			AMY120	0.0023	AMY120	4.6×10^{-8}	AMY120	2.6×10^{-6}	–	–	
Tbr1	–	–	AMY120	2.5×10^{-4}	–	–	AMY120	0.037	AMY120	0.048	–
Nfatc2	–	–	AMY120	0.039	AMY120	3.9×10^{-2}	AMY120	6.5×10^{-4}	AMY120	0.048	–
Gabpa	Challenge:Time	0.084	–	–	–	–	–	–	FCX30*	0.077	Y
Rara	–	–	FCX30	0.0372	FCX30	3.05×10^{-7}			FCX30	0.080	Y
Egr2	–	–	FCX120	0.037	FCX120	1.1×10^{-6}	–	–	FCX120*	0.011	Y
Fos	–	–	HYP30	2.0×10^{-8}	–	–	–	–	–	–	–
			HYP120	0.028	HYP120	9.6×10^{-5}					
			AMY30	0.0016	AMY30	4.5×10^{-11}					
					AMY120	1.2×10^{-6}					
Tcf7l2	–	–	HYP30	1.4×10^{-9}	HYP30	2.2×10^{-8}	–	–	–	–	–
			HYP120	6.3×10^{-16}	HYP120	2.8×10^{-8}					
			AMY120	6.3×10^{-7}	AMY120	6.5×10^{-9}					
			FCX120	1.3×10^{-7}	–	–					
Ide	Challenge	0.039	HYP30	5.5×10^{-5}	–	–	NA	NA	NA	NA	–
			HYP60	5.0×10^{-5}	–	–					
			HYP120	8.2×10^{-6}	–	–					
			AMY30	0.0031	AMY30	1.1×10^{-5}					
			AMY120	3.5×10^{-8}							
			–	–	FCX30	2.5×10^{-7}					
			FCX120	0.011	FCX20	1.2×10^{-6}					
Pomc	Tissue:Challenge:Time	6.8×10^{-4}	HYP30	1.4×10^{-9}	–	–	NA	NA	NA	NA	Y
	Tissue:Challenge	7.2×10^{-4}	HYP60	8.8×10^{-5}	–	–					
			HYP120	0.0071	HYP120	8.9×10^{-5}					

For each genomics data source and analysis—differentially expressed genes (DEGs), differential accessibility peaks (DAPs), transcriptional regulatory network (TRN) target enrichment, and motif enrichment analysis—significant results and *P*-values are reported.

[a]For genes associated with multiple DAPs in a particular brain region and time point, the lowest *P*-value is shown.

[b]Enrichment in DEG promoter-associated regions (−5 kb, +2 kb) except entries marked by asterisk, which are enriched in DAP-DEG regions.

[c]Abbreviation for brain region, followed by time (in minutes) after challenge; NA = not applicable.

[d]"All" identifies enrichment across all time points or across brain regions at a time point (for details, see Supplemental Table S11).

CNPase-positive cytoplasm (arrow in Fig. 6B); ESRRA also contained CNPase[+] cytoplasm, including processes extending from these cells. However, a number of large ESRRA[+], CNPase[−] nuclei were also found in the same regions (blue arrows in Fig. 6B,C). These large nuclei correspond to neurons, as evidenced by costaining with neuronal marker NeuN (green arrows in Fig. 6D,E). Together these data place ESRRA protein in oligodendrocytes as well as neurons in the cortex, suggesting that the protein serves regulatory functions in both types of cells.

Discussion

We describe a rich data set documenting gene expression and chromatin modulation in the mouse brain as animals respond to a salient social challenge in the form of a territorial threat. It is well known that threatened animals adjust their behavior after exposure to such a challenge (Fernald and Maruska 2012), and our goal was to develop a novel view of sequence of molecular events that direct this behavioral modulation. To do this, we measured the changing patterns of gene expression and chromatin profiles across the brain and over time and integrated these data to develop new insights to the regulatory mechanisms underlying a very complex biological response.

The completed analysis supports and significantly elaborates a model first suggested in our earlier study (Rittschof et al. 2014), in which social challenge induces a rapid shift in energy metabolism that is linked to activation of developmental signals driving neural plasticity in the brain. Here, we demonstrate that the energy shift is correlated primarily with glia, particularly oligodendrocytes, in this behavioral context and that the metabolic signal in these cells prefigures TRN activation, primarily in AMY neurons. Significant
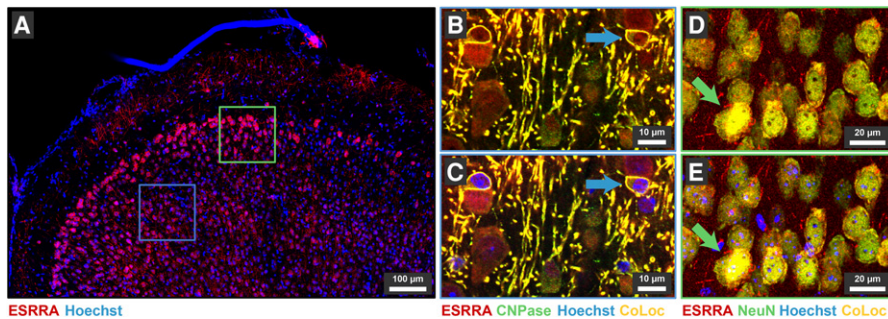
Figure 6. Localization of ESRRA. (*A*) Sagittal overview showing FCX distribution of ESRRA protein (red) with nuclei counterstained by Hoechst 33342 (blue). Blue and green boxes show approximate positions of panels *B*,*C* and *D*,*E*, respectively. (*B*,*C*) Fine detail in the FCX showing colocalization of ESRRA (red) and CNPase (green) in individual oligodendrocytes (blue arrow) without (*B*) and with (*C*) nuclear counterstain (blue). (*D*,*E*) Fine detail in the FCX showing costaining of ESRRA (red) and NeuN (green) in individual neurons (green arrow) without (*D*) and with (*E*) nuclear counterstain (blue).

shifts in chromatin accessibility over time and across the brain, particularly affecting regulatory elements that are far distal from the TSS of nearest genes, are correlated with these events. TRN reconstruction and motif enrichment highlight the underlying network of interacting TFs, including many with known functions in energy homeostasis and neurodevelopment, and estrogen-related receptor alpha is highlighted for an early, central role. We show that ESRRA, which is expressed in both cortical oligodendrocytes and neurons, binds to energy homeostasis-related and TF genes in the FCX of challenged resident mice. Since ESRRA was also implicated in our cross-species analysis of the response to territorial threat (Rittschof et al. 2014), we propose ESRRA as a central node in a gene network coupling metabolic signaling with neuronal and behavioral plasticity in the context of social threat across a diverse array of animal species.

More specifically, these data provide new information about the traverse of these events across the brain over time. The deeply conserved metabolic signal observed rapidly after challenge (Rittschof et al. 2014) is known in honey bees to represent a shift in the balance of glucose metabolism away from oxidative phosphorylation and toward aerobic glycolysis, better known as the Warburg effect (Chandrasekaran et al. 2015). Warburg metabolism has been linked to learning in other contexts, including adaptive motor learning in mice (Shannon et al. 2016). An interesting corollary to this linkage is that glycolytic "hotspots" in the adult human brain—which are also hotspots of plasticity—display "transcriptional neoteny," or gene expression patterns characteristic of the developing brain (Goyal et al. 2014). Thus, Warburg metabolism correlates with reawakening of genes associated with neuron differentiation and plasticity both spatially and temporally. Although astrocytes are a primary source of glycolytic activity in mammalian brains, other cell types, including neurons and oligodendrocytes, are sensitive to blood glucose levels and respond to other signals of metabolic state (Gundersen et al. 2015). Our study points to oligodendrocytes as the site of a Warburg-like metabolic shift and suggests that this shift is translated through metabolically-sensitive signaling pathways and TFs to neurons, activating the neotenous, plastic state.

Outlining the mechanism in further detail, our data reveal an early burst of neuropeptide signaling, very likely responsible for the metabolic shift, which is accompanied by calcium channel and neurotransmitter-related activity in the HYP and FCX. This initial phase is followed temporally by significant up-regulation of "neo-

tenous" neurodevelopmental signaling genes, particularly in the AMY. Underlying this entire sequence of events, the modeling results revealed the persistent modulation of oxidative phosphorylation as the most robust system-wide transcriptional response. Therefore, we conclude that the down-regulation of oxidative phosphorylation-related genes we detected at an early time point (Rittschof et al. 2014), driven rapidly after challenge by neural signaling and neuropeptide release, has an enduring effect in the form of plasticity that follows social challenge response across the brain.

Second, we present new information regarding the *cis-* and *trans-*acting components that regulate these processes. The response to challenge is marked by a substantial level of global chromatin reorganization, with chromatin dynamics correlating strongly with overall patterns of gene expression across the brain. Unlike an earlier study focused on response to foot shock (Halder et al. 2016), we detected a global reorganization of chromatin in response to social challenge, even at the earliest time point. Although chromatin structure is generally thought to be stable in adult cells (Whitney et al. 2014), recent work shows that activity-dependent chromatin remodeling happens in neurons within an hour (Yang et al. 2016). Our data suggest that the chromatin landscape is altered very quickly in the adult brain after a salient emotional experience. Based upon data from AMY, where early differential accessibility appears to predict late differential expression, we conclude that differential chromatin accessibility may prefigure differential expression. The differentially accessible peaks we identified were enriched in motifs associated with pioneer factors and chromatin modifiers, suggesting an important role for these factors in determining social response; the fact that most DAPs were located far from TSS suggests the importance of three-dimensional chromatin architecture in this epigenetic process. In addition to known enhancers, these DAPs comprise a rich resource of novel candidate regulatory elements that are linked to social behavior by this study for the first time.

By using network-based and motif-enrichment tools, we predicted a cohort of coordinated TFs to interact with these novel regulatory elements to drive the transcriptional response. The TRN comprises TFs known to integrate metabolic and neurobiological functions, including the estrogen-related receptor ESRRA. ESRRA itself was not differentially expressed in this study, and the ESRRA motif was enriched near baseline but not differential accessibility peaks. Yet, *Esrra* expression, ESRRA motif enrichment, and ESRRA ChIP-seq peaks strongly predict the differential expression of other genes. These facts pose a puzzle on first consideration, but they are reconciled by the nature of this TF protein and its known modes of action. In particular, ESRRA is a nuclear receptor, the activity of which is regulated through ligand binding and post-translational modifications that impact nuclear localization and DNA binding properties (Ozcan et al. 2010). Indeed, many TFs, including some of those in our network, are known to be regulated by post-translational events that affect their localization, DNA binding, protein–protein interactions, and more (e.g., Reich and Liu 2006; Ivanova et al. 2007; Ozcan et al. 2010; Boldingh Debernard et al. 2012; Dayalan Naidu and

Dinkova-Kostova 2017); TFs of this type thus need not to be significantly differentially expressed, or permitted de novo access to differentially accessible chromatin sites, to carry out differential regulatory roles.

Consistent with ChIP results in other tissues (Dufour et al. 2007; Charest-Marcotte et al. 2010), ESRRA binds primarily near genes involved in energy metabolism in cortical cells and is enriched near challenge-related DEGs. However, ESRRA binding sites are also enriched near TF genes, including key neurodevelopmental regulators, suggesting one possible mechanism through which metabolic and neurodevelopmental components of social challenge response might be transcriptionally coordinated. Known functions of *ESRRA* are consistent with this proposed role. Specifically, mouse *Esrra* mutations are associated with defects in insulin and glucose homeostasis as well as behavioral rigidity and social deficits (Luo et al. 2003; Dufour et al. 2011; Cui et al. 2015), and in human patients, *ESRRA* is linked to the combined metabolic and behavioral symptoms of eating disorders (Cui et al. 2013). On the cellular level, ESRRA regulates Warburg-like metabolic shifts in cancer cells and during cellular differentiation in mammals (Nie and Wong 2009; Charest-Marcotte et al. 2010) and coordinates a Warburg shift that is essential to *Drosophila* development (Tennessen et al. 2011). Together these data argue that ESRRA is an essential component in coordinating Warburg-like metabolism, developmental functions, and behavioral plasticity across the evolutionary spectrum.

It is not known how Warburg metabolism interfaces with neural plasticity, but two general hypotheses have been advanced. First, the redeployment of glycolysis characteristic of the Warburg response increases synthesis of raw materials like lipids, amino acids, and nucleotides. In cancer and development, these materials are essential to the rapid generation of new cells (for review, see Vander Heiden et al. 2009; Tech et al. 2015). In the brain, these materials would be directed toward neurite outgrowth, dendritic branching, synaptogenesis, synaptic remodeling, and myelination (Goyal et al. 2014). Alternatively or additionally, byproducts of aerobic glycolysis are shuttled between glia and neurons, interfacing with a range of signaling pathways (Yang et al. 2014; Gundersen et al. 2015; DiNuzzo 2016), which possibly include signaling cascades required to organize the raw materials into new neural structures (Agathocleous and Harris 2013).

These signaling pathways may, in turn, activate neuronal gene expression. For instance, the activities of some TFs, including ESRRA regulator and coactivator PPARGC1A, are regulated directly by metabolites and metabolic signaling (Scarpulla 2006). Beyond its role in energy homeostasis, ESRRA is known as an upstream regulator of Wnt (Auld et al. 2012), and Wnt intersects with ESRRA on both metabolic and behavioral axes. Notably, mutations in the Wnt effector, *Tcf7l2*, are associated with abnormal insulin and glucose homeostasis as well as deficits in fear learning (for review, see Nobrega 2013). *Tcf7l2* is one of a small number of genes significantly up-regulated across the brain 120 min after challenge, suggesting an important late role in challenge response. Together these data suggest a model in which Wnt and neural plasticity downstream from *Tcf7l2* is metabolically regulated through ESRRA in socially responsive regions of the brain.

We close by pointing to a clear limitation of this study: Our experiments were conducted in tissue homogenates, limiting our ability to assign expression or chromatin signals to any specific cell type. Our data, together with results of previous studies (Cui et al., 2015), assign ESRRA regulatory function primarily to neurons and oligodendrocytes in the cortex, suggesting these cells as

the locus of the metabolic shift in this specific context. However, cell-type–specific methods of discovery will be required to address this hypothesis and add further depth to the discussion. Nevertheless, we provide a novel view of the brain's response to social challenge, including a large collection of novel challenge-associated enhancers and networked TFs with predicted metabolic and neurobehavioral roles. The data build support for a deeply conserved, fundamental, and mechanistic link between shifts in brain energy metabolism and subsequent redeployment of developmental factors for behavioral plasticity in the context of emotional learning.

Methods

Animals

All protocols were approved by the UIUC IACUC (protocol no. 15245) and undertaken in compliance with the NIH Guide for the Care and Use of Laboratory Animals. All reasonable efforts were undertaken to minimize animal suffering. Briefly, after a period of habituation to our animal room and cohousing with females to establish a territory, animals were confronted with an unfamiliar intruder for 5 min and then kept in a quiet, dark place for 30, 60, or 120 min until they were euthanized by cervical dislocation. Immediately after euthanasia we extracted FCX, HYP, and AMY. A schematic of the dissection is included as Supplemental Figure S1, and detailed methods for animal husbandry, behavior, and dissections are included in Supplemental Methods.

RNA extraction and library preparation and RNA sequencing

Dissected tissue was immediately flash-frozen in liquid nitrogen and held at −80°C. Total RNA was prepared and analyzed for quality as previously described (Bolt et al. 2016). RNA-seq libraries were prepared robotically from total RNA and then sequenced on an Illumina HiSeq 2500 sequencer. Detailed methods for RNA extraction, library preparation, and RNA-seq are included in Supplemental Methods.

RNA-seq bioinformatics, functional enrichment, and WGCNA analysis

FASTQ files were aligned to the Ensembl (Flicek et al. 2012) annotation of the NCBIM37 version of the mouse genome using TopHat2 (Kim et al. 2013) and counted using HTSeq (Anders et al. 2015), and differential expression analyses were done using the Bioconductor package edgeR (Robinson et al. 2010).

To enrich for biological systems and visualize the results of the pairwise comparisons, we used enrichment and visualization techniques similar to the online tool REVIGO (Supek et al. 2011). Other systems enrichments utilized DAVID (Huang da et al. 2009a,b).

We used WGCNA (Langfelder and Horvath 2007) in signed mode to find modules of coexpressed genes across the entire data set. To visualize only the coexpression edges representing the most stable relationships, we extracted only the edges where the absolute value of correlation coefficients was >0.85 and was the same sign in every tissue. We visualized these relationships, calculated betweenness centrality, and plotted modules using Cytoscape (Shannon et al. 2003).

Detailed methods for RNA-seq bioinformatics, functional enrichment, and WGCNA analyses are included in Supplemental Methods.

RT-qPCR confirmation

RT-qPCR confirmation was performed for seven genes: *Dnajb1I*, *Ide*, *Igf2*, *Oxt*, *Pmch*, *Tcf7l2*, and *Zic1*. Primer sequences, run conditions, and results are presented in Supplemental Table S17. A comparison of results to RNA-seq is presented in Supplemental Figure S1, and complete RT-qPCR methods are included in Supplemental Methods.

Cell-type deconvolution analysis

Because brain tissue is a heterogeneous mixture of multiple distinct cell types, we used a modification of PSEA to deconvolve our samples and identify genes associated with some of the many cellular components of brain tissue (Kuhn et al. 2011). We used reference signals from astrocytes, neurons, oligodendrocytes, microglia, and endothelial cells generated in a previous RNA-seq experiment on sorted cells from adult mouse FCX (Zhang et al. 2014). Briefly, after regressing expression values on these reference signals, we used high-throughput model selection to find the best model or models, a good indicator of cell-type specificity. Details of the best models are reported in Supplemental Table S8, and detailed methods for cell-type deconvolution are included in Supplemental Methods.

TRN reconstruction

ASTRIX (Analyzing Subsets of Transcriptional Regulators Influencing eXpression) was applied to infer a TRN as previously described (Chandrasekaran et al. 2011). The predicted targets of TFs were defined as those genes that share very high mutual information with a TF and can be predicted quantitatively with high accuracy. We identified the TFs with predicted target genes most significantly enriched in DEGs at specific time points, tissues, or a combination of those parameters to identify a cohort of the TFs most predictive of challenge-associated DEG sets (Fig. 3; Supplemental Table S10). Further, we validated these TFs and targets against references TRNs from ENCODE (Stergachis et al. 2014). Details of the methods used to reconstruct the TRN are provided in Supplemental Methods.

ChIP tissue preparation, chromatin immunoprecipitation, and library preparation

After husbandry, challenge, and dissection as in the RNA-seq experiment for 30- and 120-min samples, tissue samples dissected from five animals were pooled for ChIP-seq. Briefly, nuclei were isolated, chromatin was fragmented, and a rabbit polyclonal antibody raised against acetylated histone H3 lysine 27 (Abcam ab4729) or ESRRA (Santa Cruz sc-66882) was used to precipitate chromatin. After ChIP, immunoprecipitated DNA was checked for quality and then used to prepare libraries that were sequenced with an Illumina HiSeq 2500 sequencer. Detailed methods used for ChIP-seq tissue preparation, library preparation, and sequencing are included in Supplemental Methods.

ChIP-seq bioinformatics

Sequence data were mapped with Bowtie 2 (Langmead and Salzberg 2012) to the UCSC *Mus musculus* mm9 genome and then analyzed for peaks using HOMER (Hypergeometric Optimization of Motif EnRichment, Heinz et al. 2010). Differential chromatin peaks were identified as any peaks that changed at least twofold between conditions with a significance cutoff of 1×10^{-4}.

To identify differential accessibility peaks associated with differential expression (DAP-DEGs), a chromatin domain was defined for each gene in the mouse mm9 genome. First, for each Ensembl-annotated splice variant arising from the gene, a window was defined that began 100 kb upstream of the transcription start site and ended 100 kb downstream from the transcription end site. Next, this window was truncated so that it did not intersect with any transcript of any other gene. A DAP that overlaps with any window of any transcript of a gene, along with that corresponding gene, constitutes a DAP-DEG.

Detailed methods used for ChIP-seq bioinformatics and statistics used for DAP calling are reported in Supplemental Methods.

Cis motif analysis

We used the Stubb algorithm (Sinha et al. 2003) to identify sequence segments with significant presence of a TF binding motif (position weight matrix), scanning the genome with 500-bp windows with a 250-bp shift size. To incorporate accessibility information (captured by H3K27ac ChIP-seq data), we required that the motif score of a 500-bp window be considered only if the window is deemed "accessible"; i.e., the windows either overlapped with identified H3K27ac ChIP peaks or were proximal to such peaks and had read count above input control. All such windows were assigned scores equaling their average read count, and the resulting profile of genome-wide scores was smoothed as previously described (Kazemian et al. 2013). Finally, windows scoring in the top three percentile were considered accessible. Detailed methods used for *cis* motif analysis are reported in Supplemental Methods.

Identification of motifs in DAP-DEGs

To test for *cis* motif enrichment in DAP-DEGs, we adapted the method above as follows: For each motif, the Stubb score *P*-value corresponding to the best-scoring 500-bp window that overlapped each DAP-DEG was assigned as the score of that DAP-DEG. The number of DAP-DEGs with scores <0.05 were counted and subjected to a binomial test where the success probability parameter was learned from the frequency of such motif scores in size-matched background sequences that were sampled from gene deserts and did not contain the H3K27ac mark.

Thick-slice CLARITY immunohistochemistry

To assess the cellular and subcellular localization of specific TFs, we used a CLARITY protocol modified to work on 200-µM-thick slices of brain (Chung et al. 2013). Briefly, male animals were transcardially perfused, and then brains were extracted and fixed in the perfusion solution before being sectioned in 200-µm slices on a vibrating microtome. Sections were embedded in hydrogel and then cleared overnight using electrophoretic tissue clearing. After washing, tissue was incubated with primary antibodies (ERR-alpha: Santa Cruz sc-66882; CNPase: Millipore no. MAB326) for 3 d. After three more washes, cleared tissues were incubated with fluorescent secondary for 3 d before being washed. The final wash included the nuclear counterstain Hoechst 33342. The tissue slices were then cleared in RIMS made from 70% Histodenz (Sigma no. D2158) in PBS with Triton-X100 and mounted on lifter slides before being imaged on a Zeiss LSM 710 confocal microscope. Detailed methods used for thick slice CLARITY are reported in Supplemental Methods.

Data access

The sequencing data from this study have been submitted to the NCBI Gene Expression Omnibus (GEO; http://www.ncbi.nlm.nih.gov/geo/) under accession number GSE80345.

Acknowledgments

References

Abrajano JJ, Qureshi IA, Gokhan S, Zheng D, Bergman A, Mehler MF. 2009. REST and CoREST modulate neuronal subtype specification, maturation and maintenance. *PLoS One* **4:** e7936.

Adnani L, Langevin LM, Gautier E, Dixit R, Parsons K, Li S, Kaushik G, Wilkinson G, Wilson R, Childs S, et al. 2015. Zac1 regulates the differentiation and migration of neocortical neurons via Pac1. *J Neurosci* **35:** 13430–13447.

Agathocleous M, Harris WA. 2013. Metabolism in physiological cell proliferation and differentiation. *Trends Cell Biol* **23:** 484–492.

Anders S, Pyl PT, Huber W. 2015. HTSeq: a Python framework to work with high-throughput sequencing data. *Bioinformatics* **31:** 166–169.

Audet M-C, Mangano EN, Anisman H. 2010. Behavior and pro-inflammatory cytokine variations among submissive and dominant mice engaged in aggressive encounters: moderation by corticosterone reactivity. *Front Behav Neurosci* **4:** 156.

Auld KL, Berasi SP, Liu Y, Cain M, Zhang Y, Huard C, Fukayama S, Zhang J, Choe S, Zhong W, et al. 2012. Estrogen-related receptor α regulates osteoblast differentiation via Wnt/β-catenin signaling. *J Mol Endocrinol* **48:** 177–191.

Bayle JH, Randazzo F, Johnen G, Kaufman S, Nagy A, Rossant J, Crabtree GR. 2002. Hyperphenylalaninemia and impaired glucose tolerance in mice lacking the bifunctional DCoH gene. *J Biol Chem* **277:** 28884–28891.

Besnard A, Galan-Rodriguez B, Vanhoutte P, Caboche J. 2011. Elk-1 a transcription factor with multiple facets in the brain. *Front Neurosci* **5:** 35.

Bjorkqvist K. 2001. Social defeat as a stressor in humans. *Physiol Behav* **73:** 435–442.

Boldingh Debernard KA, Mathisen GH, Paulsen RE. 2012. Differences in NGFI-B, Nurr1, and NOR-1 expression and nucleocytoplasmic translocation in glutamate-treated neurons. *Neurochem Int* **61:** 79–88.

Bolt CC, Negi S, Guimaraes-Camboa N, Zhang H, Troy JM, Lu X, Kispert A, Evans SM, Stubbs L. 2016. Tbx18 regulates the differentiation of periductal smooth muscle stroma and the maintenance of epithelial integrity in the prostate. *PLoS One* **11:** e0154413.

Breustedt J, Vogt KE, Miller RJ, Nicoll RA, Schmitz D. 2003. α1E-containing Ca²⁺ channels are involved in synaptic plasticity. *Proc Natl Acad Sci* **100:** 12450–12455.

Buonfiglio DC, Ramos-Lobo AM, Silveira MA, Furigo IC, Hennighausen L, Frazao R, Donato J Jr. 2015. Neuronal STAT5 signaling is required for maintaining lactation but not for postpartum maternal behaviors in mice. *Horm Behav* **71:** 60–68.

Chandrasekaran S, Ament SA, Eddy JA, Rodriguez-Zas SL, Schatz BR, Price ND, Robinson GE. 2011. Behavior-specific changes in transcriptional modules lead to distinct and predictable neurogenomic states. *Proc Natl Acad Sci* **108:** 18020–18025.

Chandrasekaran S, Rittschof C, Djukovic D, Gu H, Raftery D, Price N, Robinson G. 2015. Aggression is associated with aerobic glycolysis in the honey bee brain. *Genes Brain Behav* **14:** 158–166.

Charest-Marcotte A, Dufour CR, Wilson BJ, Tremblay AM, Eichner LJ, Arlow DH, Mootha VK, Giguere V. 2010. The homeobox protein Prox1 is a negative modulator of ERRα/PGC-1α bioenergetic functions. *Gene Dev* **24:** 537–542.

Chen Y, Wang Y, Erturk A, Kallop D, Jiang Z, Weimer RM, Kaminker J, Sheng M. 2014. Activity-induced Nr4a1 regulates spine density and distribution pattern of excitatory synapses in pyramidal neurons. *Neuron* **83:** 431–443.

Chung K, Wallace J, Kim SY, Kalyanasundaram S, Andalman AS, Davidson TJ, Mirzabekov JJ, Zalocusky KA, Mattis J, Denisin AK, et al. 2013. Structural and molecular interrogation of intact biological systems. *Nature* **497:** 332–337.

Cubelos B, Sebastian-Serrano A, Beccari L, Calcagnotto ME, Cisneros E, Kim S, Dopazo A, Alvarez-Dolado M, Redondo JM, Bovolenta P, et al. 2010. Cux1 and Cux2 regulate dendritic branching, spine morphology, and synapses of the upper layer neurons of the cortex. *Neuron* **66:** 523–535.

Cui H, Moore J, Ashimi SS, Mason BL, Drawbridge JN, Han S, Hing B, Matthews A, McAdams CJ, Darbro BW, et al. 2013. Eating disorder predisposition is associated with ESRRA and HDAC4 mutations. *J Clin Invest* **123:** 4706–4713.

Cui H, Lu Y, Khan MZ, Anderson RM, McDaniel L, Wilson HE, Yin TC, Radley JJ, Pieper AA, Lutter M. 2015. Behavioral disturbances in estrogen-related receptor α-null mice. *Cell Rep* **11:** 344–350.

Dayalan Naidu S, Dinkova-Kostova AT. 2017. Regulation of the mammalian heat shock factor 1. *FEBS J* doi: 10.1111/febs.13999.

Deblois G, Hall JA, Perry MC, Laganiere J, Ghahremani M, Park M, Hallett M, Giguere V. 2009. Genome-wide identification of direct target genes implicates estrogen-related receptor α as a determinant of breast cancer heterogeneity. *Cancer Res* **69:** 6149–6157.

DiNuzzo M. 2016. Astrocyte-neuron interactions during learning may occur by lactate signaling rather than metabolism. *Front Integr Neurosci* **10:** 2.

Dufour CR, Wilson BJ, Huss JM, Kelly DP, Alaynick WA, Downes M, Evans RM, Blanchette M, Giguere V. 2007. Genome-wide orchestration of cardiac functions by the orphan nuclear receptors ERRα and γ. *Cell Metab* **5:** 345–356.

Dufour CR, Levasseur MP, Pham NH, Eichner LJ, Wilson BJ, Charest-Marcotte A, Duguay D, Poirier-Heon JF, Cermakian N, Giguere V. 2011. Genomic convergence among ERRα, PROX1, and BMAL1 in the control of metabolic clock outputs. *PLoS Genet* **7:** e1002143.

Duvarci S, Pare D. 2014. Amygdala microcircuits controlling learned fear. *Neuron* **82:** 966–980.

Fernald RD, Maruska KP. 2012. Social information changes the brain. *Proc Natl Acad Sci* **109**(Suppl 2): 17194–17199.

Flicek P, Amode MR, Barrell D, Beal K, Brent S, Carvalho-Silva D, Clapham P, Coates G, Fairley S, Fitzgerald S, et al. 2012. Ensembl 2012. *Nucleic Acids Res* **40:** D84–D90.

Frullanti E, Amabile S, Lolli MG, Bartolini A, Livide G, Landucci E, Mari F, Vaccarino FM, Ariani F, Massimino L, et al. 2016. Altered expression of neuropeptides in FoxG1-null heterozygous mutant mice. *Eur J Hum Genet* **24:** 252–257.

Garretson JT, Teubner BJ, Grove KL, Vazdarjanova A, Ryu V, Bartness TJ. 2015. Peroxisome proliferator-activated receptor γ controls ingestive behavior, agouti-related protein, and neuropeptide Y mRNA in the arcuate hypothalamus. *J Neurosci* **35:** 4571–4581.

Gilmartin MR, Balderston NL, Helmstetter FJ. 2014. Prefrontal cortical regulation of fear learning. *Trends Neurosci* **37:** 455–464.

Goyal MS, Hawrylycz M, Miller JA, Snyder AZ, Raichle ME. 2014. Aerobic glycolysis in the human brain is associated with development and neotenous gene expression. *Cell Metab* **19:** 49–57.

Graef IA, Wang F, Charron F, Chen L, Neilson J, Tessier-Lavigne M, Crabtree GR. 2003. Neurotrophins and netrins require calcineurin/NFAT signaling to stimulate outgrowth of embryonic axons. *Cell* **113:** 657–670.

Gundersen V, Storm-Mathisen J, Bergersen LH. 2015. Neuroglial transmission. *Physiol Rev* **95:** 695–726.

Halder R, Hennion M, Vidal RO, Shomroni O, Rahman RU, Rajput A, Centeno TP, van Bebber F, Capece V, Vizcaino JC, et al. 2016. DNA methylation changes in plasticity genes accompany the formation and maintenance of memory. *Nat Neurosci* **19:** 102–110.

Hawker DS, Boulton MJ. 2000. Twenty years' research on peer victimization and psychosocial maladjustment: a meta-analytic review of cross-sectional studies. *J Child Psychol Psychiatry* **41:** 441–455.

Heinz S, Benner C, Spann N, Bertolino E, Lin YC, Laslo P, Cheng JX, Murre C, Singh H, Glass CK. 2010. Simple combinations of lineage-determining transcription factors prime *cis*-regulatory elements required for macrophage and B cell identities. *Mol Cell* **38:** 576–589.

Hoffmann A, Spengler D. 2012. Transient neonatal diabetes mellitus gene *Zac1* impairs insulin secretion in mice through Rasgrf1. *Mol Cell Biol* **32:** 2549–2560.

Hon GC, Hawkins RD, Ren B. 2009. Predictive chromatin signatures in the mammalian genome. *Hum Mol Genet* **18:** R195–R201.

Huang da W, Sherman BT, Lempicki RA. 2009a. Bioinformatics enrichment tools: paths toward the comprehensive functional analysis of large gene lists. *Nucleic Acids Res* **37:** 1–13.

Huang da W, Sherman BT, Lempicki RA. 2009b. Systematic and integrative analysis of large gene lists using DAVID bioinformatics resources. *Nat Protoc* **4:** 44–57.

Huang TN, Chuang HC, Chou WH, Chen CY, Wang HF, Chou SJ, Hsueh YP. 2014. Tbr1 haploinsufficiency impairs amygdalar axonal projections and results in cognitive abnormality. *Nat Neurosci* **17:** 240–247.

Hung HC, Hsiao YH, Gean PW. 2015a. Learning induces sonic hedgehog signaling in the amygdala which promotes neurogenesis and long-term memory formation. *Int J Neuropsychopharmacol* **18:** pyu071.

Hung HC, Hsiao YH, Gean PW. 2015b. Sonic hedgehog signaling regulates amygdalar neurogenesis and extinction of fear memory. *Eur Neuropsychopharmacol* **25:** 1723–1732.

Huss JM, Garbacz WG, Xie W. 2015. Constitutive activities of estrogen-related receptors: transcriptional regulation of metabolism by the ERR pathways in health and disease. *Biochim Biophys Acta* **1852:** 1912–1927.

Ivanova IA, Vespa A, Dagnino L. 2007. A novel mechanism of E2F1 regulation via nucleocytoplasmic shuttling: determinants of nuclear import and export. *Cell Cycle* **6:** 2186–2195.

Iwafuchi-Doi M, Zaret KS. 2014. Pioneer transcription factors in cell reprogramming. *Genes Dev* **28:** 2679–2692.

Joo JY, Schaukowitch K, Farbiak L, Kilaru G, Kim TK. 2016. Stimulus-specific combinatorial functionality of neuronal c-fos enhancers. *Nat Neurosci* **19:** 75–83.

Kazemian M, Pham H, Wolfe SA, Brodsky MH, Sinha S. 2013. Widespread evidence of cooperative DNA binding by transcription factors in *Drosophila* development. *Nucleic Acids Res* **41:** 8237–8252.

Kim D, Pertea G, Trapnell C, Pimentel H, Kelley R, Salzberg SL. 2013. TopHat2: accurate alignment of transcriptomes in the presence of insertions, deletions and gene fusions. *Genome Biol* **14:** R36.

Kuhn A, Thu D, Waldvogel HJ, Faull RL, Luthi-Carter R. 2011. Population-specific expression analysis (PSEA) reveals molecular changes in diseased brain. *Nat Methods* **8:** 945–947.

Laganiere J, Tremblay GB, Dufour CR, Giroux S, Rousseau F, Giguere V. 2004. A polymorphic autoregulatory hormone response element in the human estrogen-related receptor α (ERRα) promoter dictates peroxisome proliferator-activated receptor γ coactivator-1α control of ERRα expression. *J Biol Chem* **279:** 18504–18510.

Langfelder P, Horvath S. 2007. Eigengene networks for studying the relationships between co-expression modules. *BMC Syst Biol* **1:** 54.

Langmead B, Salzberg SL. 2012. Fast gapped-read alignment with Bowtie 2. *Nat Methods* **9:** 357–359.

Lee SC, Choi S, Lee T, Kim HL, Chin H, Shin HS. 2002. Molecular basis of R-type calcium channels in central amygdala neurons of the mouse. *Proc Natl Acad Sci* **99:** 3276–3281.

Li SY, Huang PH, Tarng DC, Lin TP, Yang WC, Chang YH, Yang AH, Lin CC, Yang MH, Chen JW, et al. 2015. Four-and-a-half LIM domains protein 2 is a coactivator of Wnt signaling in diabetic kidney disease. *J Am Soc Nephrol* **26:** 3072–3084.

Lin CH, Hansen S, Wang Z, Storm DR, Tapscott SJ, Olson JM. 2005. The dosage of the neuroD2 transcription factor regulates amygdala development and emotional learning. *Proc Natl Acad Sci* **102:** 14877–14882.

Liu D, Zhang Z, Teng CT. 2005. Estrogen-related receptor-γ and peroxisome proliferator-activated receptor-γ coactivator-1α regulate estrogen-related receptor-α gene expression via a conserved multi-hormone response element. *J Mol Endocrinol* **34:** 473–487.

Luo J, Sladek R, Carrier J, Bader JA, Richard D, Giguere V. 2003. Reduced fat mass in mice lacking orphan nuclear receptor estrogen-related receptor α. *Mol Cell Biol* **23:** 7947–7956.

McKinsey GL, Lindtner S, Trzcinski B, Visel A, Pennacchio LA, Huylebroeck D, Higashi Y, Rubenstein JL. 2013. Dlx1&2-dependent expression of Zfhx1b (Sip1, Zeb2) regulates the fate switch between cortical and striatal interneurons. *Neuron* **77:** 83–98.

Meehan WP, Leedom LJ, Nagayama T, Zeidler A. 1987. Hyperglycemia and fight-flight behavior in nondiabetic and diabetic mice. *Physiol Behav* **41:** 397–403.

Murphy LL, Hughes CC. 2002. Endothelial cells stimulate T cell NFAT nuclear translocation in the presence of cyclosporin A: involvement of the wnt/glycogen synthase kinase-3 β pathway. *J Immunol* **169:** 3717–3725.

Ng HH, Zhang Y, Hendrich B, Johnson CA, Turner BM, Erdjument-Bromage H, Tempst P, Reinberg D, Bird A. 1999. MBD2 is a transcriptional repressor belonging to the MeCP1 histone deacetylase complex. *Nat Genet* **23:** 58–61.

Nie Y, Wong C. 2009. Suppressing the activity of ERRα in 3T3-L1 adipocytes reduces mitochondrial biogenesis but enhances glycolysis and basal glucose uptake. *J Cell Mol Med* **13:** 3051–3060.

Nobrega MA. 2013. TCF7L2 and glucose metabolism: time to look beyond the pancreas. *Diabetes* **62:** 706–708.

Notwell JH, Heavner WE, Darbandi SF, Katzman S, McKenna WL, Ortiz-Londono CF, Tastad D, Eckler MJ, Rubenstein JL, McConnell SK, et al. 2016. TBR1 regulates autism risk genes in the developing neocortex. *Genome Res* **26:** 1013–1022.

Ozcan S, Andrali SS, Cantrell JE. 2010. Modulation of transcription factor function by O-GlcNAc modification. *Biochim Biophys Acta* **1799:** 353–364.

Papachristou P, Dyberg C, Lindqvist M, Horn Z, Ringstedt T. 2014. Transgenic increase of Wnt7b in neural progenitor cells decreases ex-

pression of T-domain transcription factors and impairs neuronal differentiation. *Brain Res* **1576:** 27–34.

Pereverzev A, Mikhna M, Vajna R, Gissel C, Henry M, Weiergraber M, Hescheler J, Smyth N, Schneider T. 2002. Disturbances in glucose-tolerance, insulin-release, and stress-induced hyperglycemia upon disruption of the Ca(v)2.3 (α1E) subunit of voltage-gated Ca^{2+} channels. *Mol Endocrinol* **16:** 884–895.

Perez-Sieira S, Lopez M, Nogueiras R, Tovar S. 2014. Regulation of NR4A by nutritional status, gender, postnatal development and hormonal deficiency. *Sci Rep* **4:** 4264.

Pincheira R, Baerwald M, Dunbar JD, Donner DB. 2009. Sall2 is a novel p75NTR-interacting protein that links NGF signalling to cell cycle progression and neurite outgrowth. *EMBO J* **28:** 261–273.

Pittenger C. 2013. Disorders of memory and plasticity in psychiatric disease. *Dialogues Clin Neurosci* **15:** 455.

Pratt T, Tian NM, Simpson TI, Mason JO, Price DJ. 2004. The winged helix transcription factor Foxg1 facilitates retinal ganglion cell axon crossing of the ventral midline in the mouse. *Development* **131:** 3773–3784.

Reich NC, Liu L. 2006. Tracking STAT nuclear traffic. *Nat Rev Immunol* **6:** 602–612.

Rittschof CC, Bukhari SA, Sloofman LG, Troy JM, Caetano-Anollés D, Cash-Ahmed A, Kent M, Lu X, Sanogo YO, Weisner PA. 2014. Neuromolecular responses to social challenge: common mechanisms across mouse, stickleback fish, and honey bee. *Proc Natl Acad Sci* **111:** 17929–17934.

Robinson MD, McCarthy DJ, Smyth GK. 2010. edgeR: a Bioconductor package for differential expression analysis of digital gene expression data. *Bioinformatics* **26:** 139–140.

Rossi M, Colecchia D, Iavarone C, Strambi A, Piccioni F, Verrotti di Pianella A, Chiariello M. 2011. Extracellular signal-regulated kinase 8 (ERK8) controls estrogen-related receptor α (ERRα) cellular localization and inhibits its transcriptional activity. *J Biol Chem* **286:** 8507–8522.

Sakkou M, Wiedmer P, Anlag K, Hamm A, Seuntjens E, Ettwiller L, Tschop MH, Treier M. 2007. A role for brain-specific homeobox factor Bsx in the control of hyperphagia and locomotory behavior. *Cell Metab* **5:** 450–463.

Savage DB, Agostini M, Barroso I, Gurnell M, Luan J, Meirhaeghe A, Harding AH, Ihrke G, Rajanayagam O, Soos MA, et al. 2002. Digenic inheritance of severe insulin resistance in a human pedigree. *Nat Genet* **31:** 379–384.

Scarpulla RC. 2006. Nuclear control of respiratory gene expression in mammalian cells. *J Cell Biochem* **97:** 673–683.

Schwab MH, Bartholomae A, Heimrich B, Feldmeyer D, Druffel-Augustin S, Goebbels S, Naya FJ, Zhao S, Frotscher M, Tsai MJ, et al. 2000. Neuronal basic helix-loop-helix proteins (NEX and BETA2/Neuro D) regulate terminal granule cell differentiation in the hippocampus. *J Neurosci* **20:** 3714–3724.

Scobie KN, Hall BJ, Wilke SA, Klemenhagen KC, Fujii-Kuriyama Y, Ghosh A, Hen R, Sahay A. 2009. Kruppel-like factor 9 is necessary for late-phase neuronal maturation in the developing dentate gyrus and during adult hippocampal neurogenesis. *J Neurosci* **29:** 9875–9887.

Shannon P, Markiel A, Ozier O, Baliga NS, Wang JT, Ramage D, Amin N, Schwikowski B, Ideker T. 2003. Cytoscape: a software environment for integrated models of biomolecular interaction networks. *Genome Res* **13:** 2498–2504.

Shannon BJ, Vaishnavi SN, Vlassenko AG, Shimony JS, Rutlin J, Raichle ME. 2016. Brain aerobic glycolysis and motor adaptation learning. *Proc Natl Acad Sci* **113:** E3782–E3791.

Sinha S, van Nimwegen E, Siggia ED. 2003. A probabilistic method to detect regulatory modules. *Bioinformatics* **19**(Suppl 1): i292–i301.

Spaapen F, van den Akker GG, Caron MM, Prickaerts P, Rofel C, Dahlmans VE, Surtel DA, Paulis Y, Schweizer F, Welting TJ, et al. 2013. The immediate early gene product EGR1 and polycomb group proteins interact in epigenetic programming during chondrogenesis. *PLoS One* **8:** e58083.

Stergachis AB, Neph S, Sandstrom R, Haugen E, Reynolds AP, Zhang M, Byron R, Canfield T, Stehling-Sun S, Lee K. 2014. Conservation of *trans*-acting circuitry during mammalian regulatory evolution. *Nature* **515:** 365–370.

Supek F, Bošnjak M, Škunca N, Šmuc T. 2011. REVIGO summarizes and visualizes long lists of gene ontology terms. *PLoS One* **6:** e21800.

Suzuki DE, Ariza CB, Porcionatto MA, Okamoto OK. 2011. Upregulation of E2F1 in cerebellar neuroprogenitor cells and cell cycle arrest during postnatal brain development. *In Vitro Cell Dev Biol Anim* **47:** 492–499.

Takahashi A, Miczek KA. 2014. Neurogenetics of aggressive behavior: studies in rodents. *Curr Top Behav Neurosci* **17:** 3–44.

Tech K, Deshmukh M, Gershon TR. 2015. Adaptations of energy metabolism during cerebellar neurogenesis are co-opted in medulloblastoma. *Cancer Lett* **356:** 268–272.

Tennessen JM, Baker KD, Lam G, Evans J, Thummel CS. 2011. The *Drosophila* estrogen-related receptor directs a metabolic switch that supports developmental growth. *Cell Metab* **13:** 139–148.

Valenta T, Lukas J, Korinek V. 2003. HMG box transcription factor TCF-4's interaction with CtBP1 controls the expression of the Wnt target Axin2/Conductin in human embryonic kidney cells. *Nucleic Acids Res* **31:** 2369–2380.

Vander Heiden MG, Cantley LC, Thompson CB. 2009. Understanding the Warburg effect: the metabolic requirements of cell proliferation. *Science (New York, NY)* **324:** 1029–1033.

Villena JA, Kralli A. 2008. ERRα: a metabolic function for the oldest orphan. *Trends Endocrinol Metab* **19:** 269–276.

Wang S, Sun Z, Zhang X, Li Z, Wu M, Zhao W, Wang H, Chen T, Yan H, Zhu J. 2015. Wnt1 positively regulates CD36 expression via TCF4 and PPAR-γ in macrophages. *Cell Physiol Biochem* **35:** 1289–1302.

Whitney O, Pfenning AR, Howard JT, Blatti CA, Liu F, Ward JM, Wang R, Audet JN, Kellis M, Mukherjee S, et al. 2014. Core and region-enriched networks of behaviorally regulated genes and the singing genome. *Science* **346:** 1256780.

Yang TT, Suk HY, Yang X, Olabisi O, Yu RY, Durand J, Jelicks LA, Kim JY, Scherer PE, Wang Y, et al. 2006. Role of transcription factor NFAT in glucose and insulin homeostasis. *Mol Cell Biol* **26:** 7372–7387.

Yang J, Ruchti E, Petit JM, Jourdain P, Grenningloh G, Allaman I, Magistretti PJ. 2014. Lactate promotes plasticity gene expression by potentiating NMDA signaling in neurons. *Proc Natl Acad Sci* **111:** 12228–12233.

Yang Y, Yamada T, Hill KK, Hemberg M, Reddy NC, Cho HY, Guthrie AN, Oldenborg A, Heiney SA, Ohmae S, et al. 2016. Chromatin remodeling inactivates activity genes and regulates neural coding. *Science* **353:** 300–305.

Zhang Y, Chen K, Sloan SA, Bennett ML, Scholze AR, O'Keeffe S, Phatnani HP, Guarnieri P, Caneda C, Ruderisch N. 2014. An RNA-sequencing transcriptome and splicing database of glia, neurons, and vascular cells of the cerebral cortex. *J Neurosci* **34:** 11929–11947.

Transcriptional regulatory dynamics drive coordinated metabolic and neural response to social challenge in mice

Michael C. Saul, Christopher H. Seward, Joseph M. Troy, et al.

Supplemental Material	http://genome.cshlp.org/content/suppl/2017/04/28/gr.214221.116.DC1
References	This article cites 102 articles, 32 of which can be accessed free at: http://genome.cshlp.org/content/27/6/959.full.html#ref-list-1
Creative Commons License	This article is distributed exclusively by Cold Spring Harbor Laboratory Press for the first six months after the full-issue publication date (see http://genome.cshlp.org/site/misc/terms.xhtml). After six months, it is available under a Creative Commons License (Attribution-NonCommercial 4.0 International), as described at http://creativecommons.org/licenses/by-nc/4.0/.
Email Alerting Service	Receive free email alerts when new articles cite this article - sign up in the box at the top right corner of the article or **click here.**